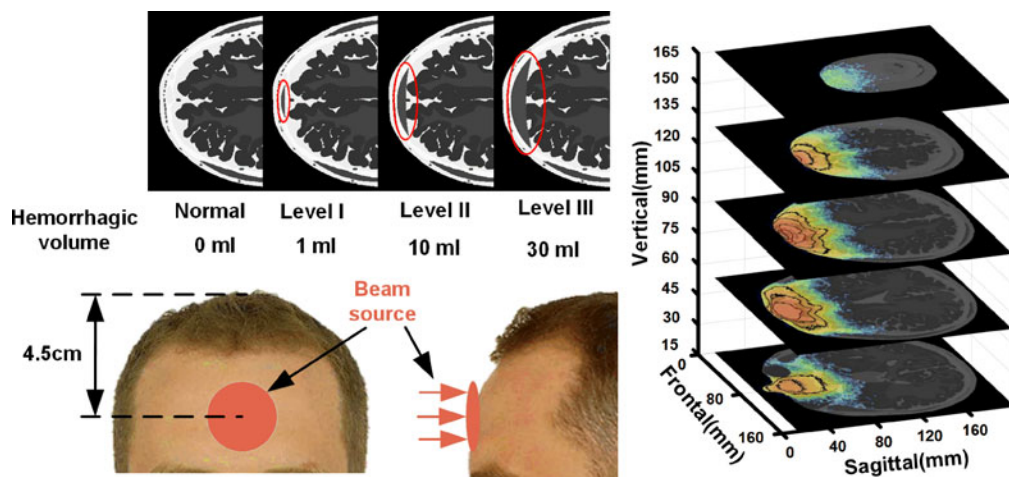# Optimize Illumination Parameter of Low-Level Laser Therapy for Hemorrhagic Stroke by Monte Carlo Simulation on Visible Human Dataset

Ting Li
Pengbo Wang
Lina Qiu
Xiang Fang
Yu Shang

Optimize Illumination Parameter of Low-Level Laser Therapy for Hemorrhagic Stroke by Monte Carlo Simulation on Visible Human Dataset

Ting Li [ID],[1,2] Pengbo Wang,[1,2] Lina Qiu,[3] Xiang Fang,[2] and Yu Shang [ID] [4]

[1]State Key Lab of Electronic Thin Films & Integrated Devices, University of Electronic Science & Technology of China, Chengdu 610054, China
[2]Chinese Academy of Medical Science and Peking Union Medical College, Institute of Biomedical Engineering, Tianjin 300192, China
[3]Dipartimento di Fisica, Politecnico di Milano, Milan 20133, Italy
[4]College of Information and Communication Engineering, North University of China, Taiyuan 030051, China

Abstract: Stroke is the second leading cause of death and disability worldwide. The incidence of hemorrhagic stroke increases dramatically with the increasingly aging population. Recently, technology of low-level light/laser therapy (LLLT) is emerging as a novel noninvasive therapeutic approach to treat stroke based on effective photobiomodulation. To obtain optimal therapeutic effects, several LLLT illumination parameters such as beam size and beam type need to be optimized. However, the quantitative optimization of LLLT illumination parameters for stroke therapeutics is impractical to test directly on human subjects. In this paper, we employed a precise voxelized three-dimensional Monte Carlo method (MCVM) to simulate photon propagation within Visible Chinese human (VCH) head at different level of stroke with varied parameters of beams. By evaluation with criteria of the total fluence flux in lesion region and the maximal penetration depth, we found that Gaussian beam with larger or the same size of hemorrhagic region generates the highest and relative homogeneous therapeutic outcomes, while the Top-hat beam performed better when hemorrhagic region is much bigger than beam size. These results demonstrate the great potential of using VCH and MCVM in optimizing LLLT treatment parameters for stroke and in guiding future instrumentation of LLLT on hemorrhagic stroke.

Index Terms: Low-level laser therapy, hemorrhagic stroke, Monte Carlo, optimization, illumination parameter, Visible Chinese human (VCH).

1. Introduction

Stroke has become the second leading cause of death and disability in adults worldwide, due to high incidence rate, high mortality rate and high disability rate [1], [2]. Thus, World Health Organization

(WHO) has set a priority for prevention and treatment of stroke. It was noted that in China, where the population of stroke patients is largest, the incidence and mortality rates of stroke are the highest. Specifically, stroke caused about more than $40 billion medical costs. Furthermore, the incidence of stroke increased by 9% annually. According to pathological mechanism, there are two types of stroke: one is ischemic stroke resulted from poor blood supply, and the other is hemorrhagic stroke caused by bleeding. The incidence of ischemic stroke is twice as hemorrhagic stroke globally (i.e., ischemic stroke: 299.1 per 100 000 people; hemorrhagic stroke: 116.6 per 100 000 people) [3]. However, the mortality rate of hemorrhagic stroke reached 63%, much higher than ischemic stroke [3], [4]. Additionally, the disability cases resulting from hemorrhagic stroke is 40% higher than that of ischemic stroke (absolute number of disability in ischemic stroke and hemorrhagic stroke populations are about 47 million and 65 million, respectively) [4]. Hence, hemorrhagic stroke is much more severe than ischemic stroke.

The major cause of hemorrhagic stroke is head injury, due primarily to accidental tumble and traffic accident [5]. Accidental tumble resulted in cerebrovascular accident (CVA), which is defined as the interruption of brain blood supply in a traumatic or non-traumatic way, subsequently impairing brain's function such as spastic hypertonia. Surgery is a standard approach that can completely remove hemorrhagic tissue, but it has risk of inducing deep psychological wounds and physical injury [6], [7]. Drug therapy is a conservative treatment, which can only ease symptoms rather than fully recover from stroke. Moreover, the drug adds the burdens on digestive organs [8], [9]. Apart from these, acupuncture, moxibustion and traditional Chinese manipulation are also the candidate therapies in China, but most of which are based on experience and always have uncertain therapeutic effects. For the therapy on hemorrhagic stroke, effective and noninvasive approaches are still rare.

In recent years, researchers found that near-infrared spectroscopy is a noninvasive and relatively inexpensive method for hemodynamic measurements [10], [11], which is also a high efficient method for stroke treatment, such as the Low Level Light Therapy (LLLT) [12]. With Low-level laser light being launched into biological cells, a large number of Adenosine Triphosphate (ATP) are generated by mitochondrion, which can increase mitochondrial activity and maintain cytochrome C oxidase activities [13]–[15]. LLLT can restore tissue function and can promote dead cells or tissues catabolism at an increasing rate, and therefore can arouse dying cells [11]. Previous studies have demonstrated the possibility of LLLT for stroke treatment, but most of these studies were performed on animals [16]–[18]. The application of LLLT for treating human stroke is few. One of the possible reasons is the difficulty in selecting the suitable illumination parameters, such as light wavelength, beam size, and beam type [19]. After reviewing the literatures on the transcranial LLLT, we found that 810 ± 20 nm light was the most common transcranial treatment light in near-infrared light. Furthermore, 810 nm not only has been demonstrated to achieve the deepest penetration through head, reaching the cerebral cortex compared with 660 nm and 980 nm [20], but was optimal for photon absorption by CCO (the peaks of light absorption: 820 nm–840 nm) [21], [22]. However, how to determine the optimal light beam (including size and type) in LLLT remains unclear for human stroke treatment. The object of this study is to find out the optimal illumination parameters of LLLT in hemorrhagic stroke treatment for human. For this purpose, we used a voxelized 3-D Monte Carlo (MCVM) simulation on visible Chinese human (VCH) head to optimize illumination parameters of LLLT for hemorrhagic stroke at different levels. MCMV has been demonstrated as a flexible and accurate simulation software [23], which is more appropriate than MCML for complex heterogeneous medium [24]. More details of MCVM were described in [22], [25], [24]. The VCH model, which is a newly developed whole-body anatomical model from high-resolution transversal photographs of a Chinese adult male cadaver, was utilized in our simulations [26]–[28]. The human body sample of VCH was specifically selected to match the average dimension and anatomical structure of human. Numerous advantages, including high resolution, precise segmentation, and up-standing posture of human sample, make the VCH model be realistic to represent common human anatomical structure [25], [27]–[30]. VCH has been well utilized in radiation quantification [29], [30], and recently it was used for precise modeling of light propagation in human body with MCVM approach [23]–[25], [27].
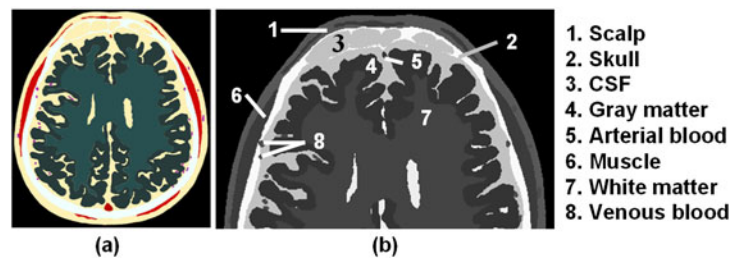
Fig. 1. VCH head model. (a) Digital color photograph of one section in the VCH head dataset; (b) Segmentation of the section in (a) with number denoting different type of tissues.

Table 1

Optical Properties of Head Tissues at 808 nm

Tissue type	μ_a (cm^{-1})	μ_s (cm^{-1})	n	g	Refs.
CSF	0.04	24	1.33	0.90	[31]
Scalp	0.18	190	1.37	0.81	[31,32]
Skull	0.16	160	1.43	0.90	[31,32]
Muscle	1.4	500	1.4	0.90	[12,25]
Gray matter	0.36	220	1.37	0.90	[31,32]
White matter	0.14	910	1.37	0.90	[31,32]
Arterial blood	2.33	500	1.4	0.99	[12,25]
Venous blood	2.38	522	1.4	0.99	[12,24]

In this study, simulations were performed in a normal status of head (i.e., the original VCH head without stroke) and three head states with different levels of subdural hemorrhage created through manipulations on VCH model (more details can be found in Section 2.1). In each model, two beam sizes (beam diameter: 1 cm, 2 cm) and two beam types (Top-hat and Gaussian) were adopted. By investigation of the photon penetration path and the total fluence flux in lesion region, we found that Gaussian beam was the optimal beam type when the size of hemorrhagic region is similar or smaller than beam size. By contrast, the Top-hat beam performed better than Gaussian beam when hemorrhagic region size is much bigger than beam size.

2. Materials and Methods

2.1 Visible Chinese Human Head Model With Hemorrhage Stroke

Visible Chinese Human head model was obtained from serial sections of the whole body, which presents less sectional data loss. In addition, VCH achieves a higher resolution (0.01 cm) than that of the Visible Human Project. In our study, the normal VCH head model was divided into eight types of tissue, including scalp, skull, Cerebrospinal Fluid (CSF), gray matter, arterial blood, muscle, white matter and venous blood. As shown in Fig. 1(b), different types of tissue were labeled with different number and classified by different colors. To speed up the simulation, segmentation datasets were compressed by merging every four continuous pixels from the centered elements. Thus, the tissue model labeled with different type was resized to $0.04 \times 0.04 \times 0.04 \, \text{cm}^3$ for each voxel, resulting in a three-dimensional matrix dataset containing $455 \times 500 \times 250$ voxels. The optical properties of different head tissue at 808 nm wavelength are listed in Table 1. Here, parameter μ_a is the absorption coefficient, μ_s is the scattering coefficient, n is the refraction index of the media, and g is the anisotropy factor.

Numerous evidences show that an accidental falling is the main cause of hemorrhagic stroke [1], [5], because it leads to the bursts of an artery in the brain and fills the area with blood in
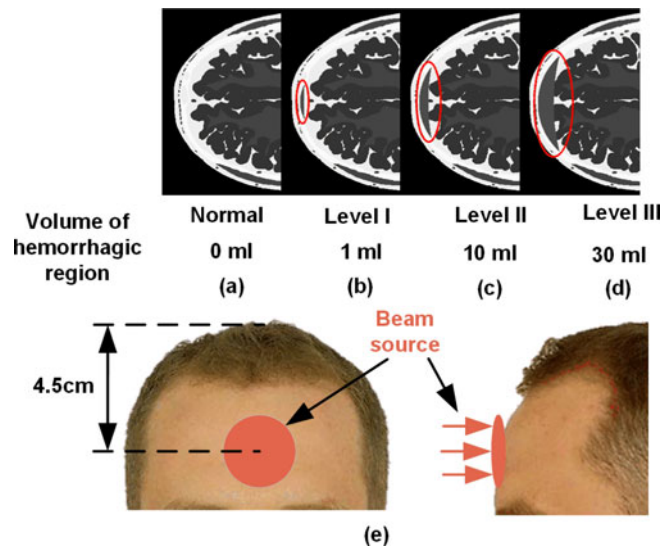
Fig. 2. The simulation setting and VCH head models (a) one slice of normal; (b)–(d) the slice of head model with the level I -III hemorrhagic region; (e) the placement of the light source.

cerebral subdural of forehead. The shape of hemorrhagic region is crescent and the component of hemorrhagic region is assumed as venous blood in the first period (e.g., the first five days or more). The severity of hemorrhagic stroke disease is proportional to the size of hemorrhagic region. In general, a blood clot of less than 1 ml causes mild headache; 10 ml causes severe headache and silent stroke, and more than 30 ml causes stroke and increase the risk of the blood clot breakage that can lead to death [33]. The VCH model was constructed from a healthy adult man. In order to depict different level of pathologic alternation in hemorrhagic stroke, we mimicked three levels of hemorrhagic stroke with different size of hemorrhagic region based on the VCH model, as shown in Fig. 2(a)–(d). We transformed the CSF or gray matter into venous by changing the color (i.e., type label) of crescent hemorrhagic region in cerebral subdural of forehead and calculated the volume of hemorrhagic region. The hemorrhagic region was manually modified in order to meet the actual status. Specifically, the volume of hemorrhagic region was $0\,cm^3$ (Normal), $0.96\,cm^3$ (level I, width $\times$ height $\times$ thickness: 2.1 cm $\times$ 2.1 cm $\times$ 0.47 cm), $9.58\,cm^3$ (level II: 5.2 cm $\times$ 5.2 cm $\times$ 0.64 cm), and $29.4\,cm^3$ (level III: 7.5 cm $\times$ 6.2 cm $\times$ 1.12 cm), respectively. The center of hemorrhagic region is always in line with the center of beam sources and the whole region is kept below the forehead subdural.

2.2 Simulation Procedure

In the simulation, the light source was placed on the center of forehead, and the incident light was injected into the tissue from the direction perpendicular to the surface (shown in Fig. 2(e)). In total, 16 simulations were performed, i.e., 2 (beam types: Gaussian beam and Top-hat beam) $\times$ 2 (beam radius: 1 cm and 2 cm) $\times$ 4 (VCH model: the normal, level I, level II, and level III). The launched photon number was 10^7 in each simulation. Each simulation was repeated five times to obtain accurate distribution profile of light fluence as well as its variation with penetration depth.

3. Results

3.1 Light Propagation

The results of fluence distribution from different head models (i.e., different illumination parameters) are shown in Fig. 3, including all 16 simulation results. The output file of MCVM contains the
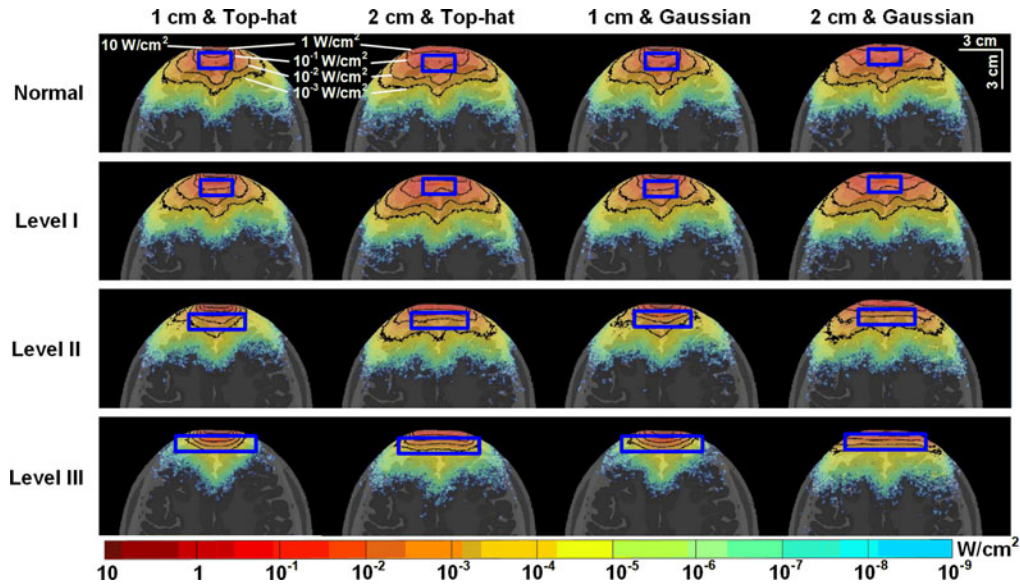
Fig. 3. The distributions of light fluence with different beam sizes and beam types in the normal and level I to level III models of hemorrhagic stroke, respectively (The radiation intensity was in a normalized pattern).

information of matrix $A(\vec{r}_s, \vec{r}_i)$, which represents the light absorption. Parameter $\mu_a(\vec{r}_i)$ is absorption coefficient (shown in Table 1). The fluence value within every voxel was calculated by (1), which was explained in [12], [26]

$$F(\vec{r}_s, \vec{r}_i) = \frac{A(\vec{r}_s, \vec{r}_i)}{\mu_a(\vec{r}_i)} \tag{1}$$

Fig. 3 shows the photon density distribution, in which the black contour lines in each sub-figure indicate isohypse lines for fluence. Moreover, the region with highest fluence flux gradient was marked by a blue rectangle in each sub-figure. As shown in Fig. 3, the effect of hemorrhagic size on the penetration depth of 2-cm-radius beam is smaller than that by 1-cm-radius beam. For the same head model, the penetration depth of 2-cm-radius beam is deeper than the 1-cm-radius beam at level I and level II. This result can be explained by light scattering which is considered as the deflection of a ray from a straight path. Some photons of beam edge would converge toward a centerline, so as to improve the penetration depth.

3.2 Total Fluence Flux in Lesion Region

The results of total fluence flux at the three levels of hemorrhagic stroke with four kinds of beams are shown in Fig. 4. Interestingly, the results of total fluence flux at level I are contrary to that of level II and level III, in term of both beam type and beam size. At level I, Gaussian beam has higher values than Top-hot beam for both radiuses, while at level II and level III, Top-hat beam achieves higher values. As for beam radius, 1 cm beam always have higher fluence flux for each beam type of level I hemorrhagic stroke. By contrast, the 1 cm beam always have lower fluence flux at level II and III. In other words, at level I, Gaussian beam with 1 cm radius has the highest value among four beam combinations (1 cm Top-hat, 2 cm Top-hat, 1 cm Gaussian and 2 cm Gaussian). At level II and level III, however, Top-hat beam with 2 cm radius achieves the highest value among four beam combinations. In addition, Gaussian beam performed better than Top-hat beam with both 1 cm and 2 cm radius at level I (radius: 1.05 cm) and Top-hat beam performed better than Gaussian beam with both 1 cm and 2 cm radius at level II (radius: 2.6 cm). When comparing
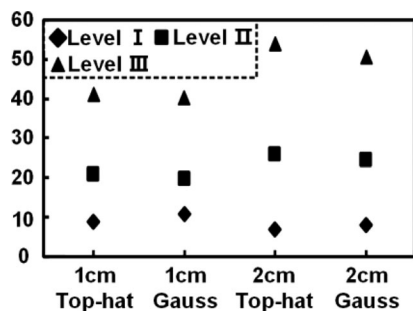
Fig. 4. The total fluence flux in lesion region at level I to level III, with different simulation.
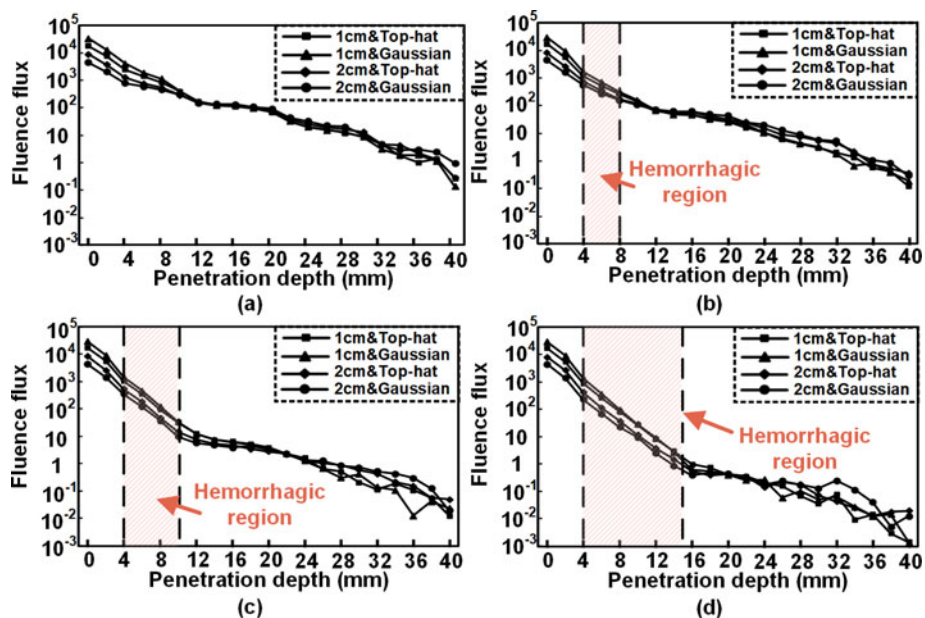

Fig. 5. The relations between fluence flux and penetration depth at different simulation schemes: (a) normal model; (b) level I model; (c) level II model; and (d) level III model. In each subfigure, the red-shaded region denotes the hemorrhagic region.

the beam size (radius) and the lesion size (radius), we found that Gaussian beam with larger or similar size of hemorrhagic region generates higher and relative more homogeneous therapeutic outcomes, while the Top-hat beam performed better when hemorrhagic region is much bigger than beam size.

3.3 Penetration Depth

The relations between the fluence flux and penetration depth for different beam combinations are shown in Fig. 5. In the hemorrhagic region (i.e., the red-shaded region in Fig. 5(b)–(d)), the slopes of fluence flux versus penetration depth in all cases were found to be quite similar ($k = -0.49 \pm 0.01$). In all polyline, the tissue with the largest declining rate is the hemorrhage-tissue, wherein the photons are strongly absorbed and reflected. Based on Fig. 5, we further calculated the maximal penetration depth for 16 simulations (assigning 1 to the fluence flux value at the maximal penetration depth) and listed in Table 2. Obviously, the maximal penetration depth declined sharply with the increase of hemorrhagic region.

Table 2

The Maximal Penetration Depth for Normal, Level I to Level III Head Models

Beam style	Normal (cm)	Level I(cm)	Level II(cm)	Level III(cm)
1cm & Top-hat	3.9956	3.3414	2.4777	1.5439
1cm & Gaussian	3.8675	3.4781	2.5043	1.5935
2cm & Top-hat	3.7924	3.6615	2.7190	1.3743
2cm & Gaussian	3.8323	3.5482	2.6843	1.4811

4. Conclusion and Discussions

We dedicated to explore the optimal illumination parameters of LLLT (e.g., beam size and beam type) for stroke treatment, we used Monte Carlo approach to simulate light propagation within the VCH models at different level of hemorrhagic stroke, and varied laser/light beam size and beam type. Totally 16 simulations were performed, i.e., 2 (beam types: Gaussian beam and Top-hat beam) × 2 (beam radius: 1 cm, 2 cm) × 4 (VCH model: normal, level I, level II and level III). By comparing the total fluence flux, we found that Gaussian beam is a more effective light source for treatment when the beam size is larger (or similar) than the hemorrhagic region. On the contrary, the Top-hat beam is more effective when the beam size is small than the hemorrhagic region.

In realistic human head model, we found that the maximal penetration of Top-hat beams was close at 2 cm-radius in normal and level I head model (as shown in Table 2). When hemorrhagic region radius is smaller than beam radius, the scattering of photons mostly occur in beam edge, will thus not be absorbed or not traveled through hemorrhagic region, subsequently reducing the penetration depth. Hence the maximal penetration of Top-hat beam is less susceptible to hemorrhagic region in the case that beam size is larger than hemorrhagic region. Besides, there was a max-limit of depth (about 4 cm) for the LLLT to effectively treat the stroke according to the simulation. It was unwise to accumulate the treatment dosage deep through enhancing treatment time or irradiation intensity. The excessive irradiation energy or too long treatment time resulted in the shallower tissue absorbing too much energy, which lead to temperature rapidly rising and tissue damage in the shallower tissue. But Bessel beam, which effectively improved the penetration depth of light, could solve this problem. Or, a multiple-light-sources illumination scheme, which were used commercially, was another available solution.

At level I, Gaussian beam with 1-cm radius obtains the largest fluence value. By contrast, level II and level III show higher fluence when using 2 cm-radius Top-hat beam. It may due to the relative size between the beam and hemorrhagic region, as well as the difference of photon density between Top-hat beam and Gaussian beam. When hemorrhagic region is smaller, photons need to migrate as wide as possible to obtain maximal fluence flux. In the case that hemorrhagic region is much larger than beam size, photons should migrate as deep as possible to obtain maximal fluence flux. With the growth in hemorrhagic region, however, the increasing rate of lesion' width and height are faster than thickness. Therefore, the photons being deflected sideway are more valuable than the photons moving straight. With the increase of lesion region, the total influence flux induced by Top-hat beam increases more rapidly than Gaussian beam. Apparently, the Gaussian beam with the same size of hemorrhagic region generates the best illumination effect, i.e., the deeper penetration depth and more fluence distribution in hemorrhagic region. Generally, the size of beam source is physically limited by device. To best fit the head, using multiple light sources is much better. In order to depict how light migration in 3D head module, we also included the sagittal and coronal views of the 3D photon flux profile with 1 cm Gaussian beam for level I stroke (Fig. 6).

The head model we used in this study, VCH, was specifically selected to match the average dimension and anatomical structure of human with high resolution and precise segmentation, which can realistically represent common human anatomical structure [24], [27]–[30]. However, the hemorrhage stroke could occur in any location of brain, the simulations of photon penetration in cerebral subdural hemorrhage may not be sufficient. Thus, more head models with different
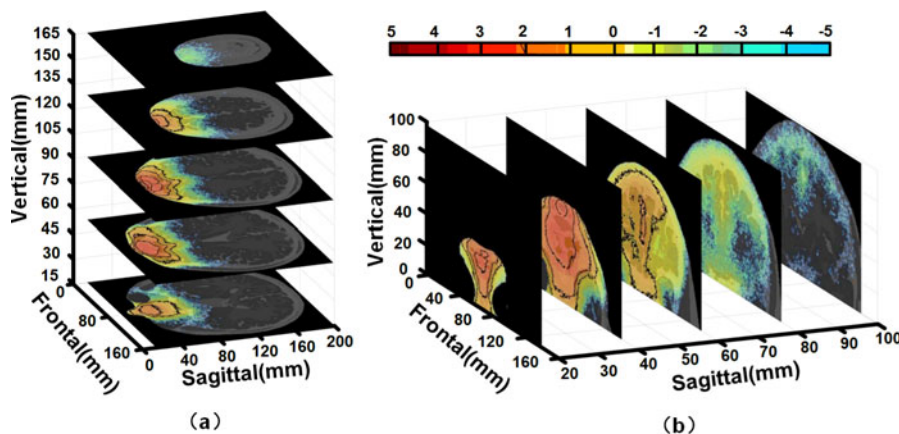
Fig. 6. The three-dimensional (3-D) light fluence distributions with 1 cm-radius Gaussian source in level I models: (a) horizontal slice views of the 3-D photon flux profile; and (b) vertical slice views of the 3-D photon flux profile.

locations of hemorrhage still need to be developed in our future work. Besides, 1064 nm light was employed more and more to transcranial LLLT. Although 1064 nm has high water absorption, the blood absorption of 1064 nm is also smaller than 800–900 nm. It is necessary to research the maximum penetration depth and the optimize illumination parameter on stroke of 1064 nm. By optimizing LLLT treatment for the stroke caused by cerebral subdural hemorrhage, we found that Gaussian beam is more proper for stroke rehabilitation, when beam size mostly covers hemorrhagic region. This finding is not only helpful for the optimization of LLLT protocol for stroke therapeutics, but also of clinical significance, particularly for aging population. Based on this study, we are now designing a multi-layered 3D-printed helmet with water-cooling, arrays of LED sources at 810 nm. Illuminating period, pulse width, and duty cycle of each LED source were remotely and independently controlled by custom-designed software. Our instrument is quite potential to be applied to clinics and research.

References

[1] E. J. Benjamin *et al.*, "Heart disease and stroke statistics-2017 update: A report from the American heart association," *Circulation*, vol. 135, no. 10, 2017, Art. no. e146-e603.

[2] A. S. Go *et al.*, "Heart disease and stroke statistics-2013 update: A report from the American heart association," *Circulation*, vol. 127, no. 23, 2013, Art. no. e6-e245.

[3] R. V. Krishnamurthi *et al.*, "The global burden of hemorrhagic stroke: A summary of findings from the GBD 2010 study," *Global Heart*, vol. 9, no. 1, pp. 101–106, 2014.

[4] Feigin, "Update on the global burden of ischemic and hemorrhagic stroke in 1990-2013: The GBD 2013 study," *Neuroepidemiology*, vol. 48, no. 1-2, pp. 86–86, 2017.

[5] Y. Y. Huang and M. R. Hamblin, "Low level laser therapy for traumatic brain injury," *Proc. SPIE Int. Soc. Opt. Eng.*, vol. 7552, no. 1, pp. 151–154, 2010.

[6] G. Wong, D. Warner, K. Offord, M. Warner, P. Maxson, and J. Whisnant, "Risk of surgery and anesthesia for ischemic stroke," *Anesthesiology*, vol. 92, no. 2, pp. 425–432, 2000.

[7] D. G. E. Mead, H. Murray, A. Farrell, P. A. O'Neill, and C. N. Mccollum, "Pilot study of carotid surgery for acute stroke," *Brit. J. Surgery.*, vol. 84, no. 7, pp. 990–992, 2010.

[8] J. D. Keyser, G. Sulter, and P. G. Luiten, "Clinical trials with neuroprotective drugs in acute ischaemic stroke: are we doing the right thing?," *Trends Neurosci.*, vol. 23, no. 6, pp. 245–246, 1999.

[9] E. Sena, H. B. V. D. Worp, D. Howells, and M. Macleod, "How can we improve the pre-clinical development of drugs for stroke?," *Trends Neurosci.*, vol. 30, no. 9, pp. 433–439, 2007.

[10] K. Li, T. Li, Y. Li, and Y. Lin, "Significant and sustaining elevation of blood oxygen induced by Chinese cupping therapy as assessed by near-infrared spectroscopy," *Biomed. Opt. Exp.*, vol. 8, no. 1, pp. 223–229, 2017.

[11] T. Li, M. Duan, L. Kai, G. Yu, and Z. Ruan, "Bedside monitoring of patients with shock using a portable spatially-resolved near-infrared spectroscopy," *Biomed. Opt. Exp.*, vol. 6, no. 9, pp. 3431–3436, 2015.

[12] L. Wu, Y. Lin, and T. Li, "Effect of human brain edema on light propagation: A Monte Carlo modeling based on the Visible Chinese Human Dataset," *IEEE Photon. J.*, vol. 9, no. 5, Oct. 2017, Art. no. 6101810.

[13] F. Schiffer *et al.*, "Psychological benefits 2 and 4 weeks after a single treatment with near infrared light to the forehead: a pilot study of 10 patients with major depression and anxiety," *Behavioral Brain Functions*, vol. 5, no. 1, pp. 46–46, 2009.

[14] X. Wang, F. Tian, S. S. Soni, F. Gonzalezlima, and H. Liu, "Interplay between up-regulation of cytochrome-c-oxidase and hemoglobin oxygenation induced by near-infrared laser," *Sci. Rep.*, vol. 6, 2016, Art. no. 30540.

[15] X. Wang *et al.*, "Up-regulation of cerebral cytochrome-c-oxidase and hemodynamics by transcranial infrared laser stimulation: A broadband near-infrared spectroscopy study," *J. Cereb. Blood Flow Metab.*, vol. 37, no. 12, pp. 3789–3802, 2017.

[16] P. A. Lapchak, K. F. Salgado, C. H. Chao, and J. A. Zivin, "Transcranial near-infrared light therapy improves motor function following embolic strokes in rabbits: An extended therapeutic window study using continuous and pulse frequency delivery modes," *Neuroscience*, vol. 148, no. 4, pp. 907–914, 2007.

[17] W. J. Xuan, T. Agrawal, L. Y. Huang, G. K. Gupta, and M. R. Hamblin, "Low-level laser therapy for traumatic brain injury in mice increases brain derived neurotrophic factor (BDNF) and synaptogenesis," (in English), *J. Biophoton.*, vol. 8, no. 6, pp. 502–511, 2015.

[18] P. A. Lapchak, J. Streeter, and L. D. Taboada, "Transcranial near infrared laser therapy (NILT) to treat acute ischemic stroke: a review of efficacy, safety and possible mechanism of action derived from rabbit embolic stroke studies," *Proc. SPIE Int. Soc. Opt. Eng.*, vol. 7552, no. 1, pp. 1–13, 2010.

[19] T. Li, Y. Zhao, Y. Sun, and K. Li, "Effects of wavelength, beam type and size on cerebral low-level laser therapy by a Monte Carlo study on visible Chinese human," *J. Innovation Opt. Health Sci.*, vol. 8, no. 01, 2015, Art. no. 1540002.

[20] T. Li, C. Xue, P. Wang, Y. Li, and L. Wu, "Photon Penetration depth in human brain for light stimulation and treatment: A Realistic Monte Carlo Simulation Study," *J. Innovative Opt. Health Sci.*, vol. 10, no. 5, 2017, Art. no. 1743002.

[21] T. I. Karu, L. V. Pyatibrat, S. F. Kolyakov, and N. I. Afanasyeva, "Absorption measurements of a cell monolayer relevant to phototherapy: reduction of cytochrome c oxidase under near IR radiation," *J. Photochem., Photobiol. B Biol.*, vol. 81, no. 2, pp. 98–106, 2005.

[22] M. Ferrari and V. Quaresima, "Review: Near infrared brain and muscle oximetry: From the discovery to current applications," *J. Near Infrared Spectroscopy*, vol. 20, no. 1, p. 1–14, 2012.

[23] T. Li, H. Gong, and Q. Luo, "MCVM: Monte Carlo modeling of photon migration in voxelized media," *J. Innovative Opt. Health Sci.*, vol. 3, no. 2, pp. 91–102, 2010.

[24] T. Li, Y. Li, Y. Sun, M. Duan, and L. Peng, "Effect of head model on Monte Carlo modeling of spatial sensitivity distribution for functional near-infrared spectroscopy," *J. Innovation Opt. Health Sci.*, vol. 8, no. 05, 2015, Art. no. 1550024.

[25] T. Li, H. Gong, and Q. Luo, "Visualization of light propagation in visible Chinese human head for functional near-infrared spectroscopy," *J. Biomed. Opt.*, vol. 16, no. 4, 2011, Art. no. 045001.

[26] Y. Shang, T. Li, L. Chen, Y. Lin, M. Toborek, and G. Yu, "Extraction of diffuse correlation spectroscopy flow index by integration of Nth-order linear model with Monte Carlo simulation," *Appl. Phys. Lett.*, vol. 104, no. 19, 2014, Art. no. 193703.

[27] S. X. Zhang *et al.*, "The Chinese Visible Human (CVH) datasets incorporate technical and imaging advances on earlier digital humans," *J. Anatomy*, vol. 204, no. 3, p. 165–173, 2004.

[28] A. A. Li, L. Qian, S. Q. Zeng, T. Lei, S. Z. Zhong, and Q. M. Luo, "Construction and visualization of high-resolution three-dimensional anatomical structure datasets for Chinese digital human," *Chin. Sci. Bull.*, vol. 53, no. 12, pp. 1848–1854, 2008.

[29] G. Zhang, Q. Luo, S. Zeng, and Q. Liu, "The development and application of the Visible Chinese Human model for Monte Carlo dose calculations," *Health Phys.*, vol. 94, no. 2, pp. 118–125, 2008.

[30] G. Zhang, Q. Liu, and Q. Luo, "Monte Carlo simulations for external neutron dosimetry based on the visible Chinese human phantom," *Phys. Med. Biol.*, vol. 52, no. 24, pp. 7367–7383, 2007.

[31] E. Okada and D. T. Delpy, "Near-infrared light propagation in an adult head model. I. Modeling of low-level scattering in the cerebrospinal fluid layer," *Appl. Opt.*, vol. 42, no. 16, pp. 2906–2914, 2003.

[32] E. Okada and D. T. Delpy, "Near-infrared light propagation in an adult head model. II. Effect of superficial tissue thickness on the sensitivity of the near-infrared spectroscopy signal," *Appl. Opt.*, vol. 42, no. 16, pp. 2915–2922, 2003.

[33] W. Z. Yang, "Study on the application of time window for activating blood circulation on hemorrhagic stroke," *Chin. J. Tradit. Chin. Med. Pharm.*, vol. 52, no. 24, pp. 743–745, 2002.